Journal of Nuclear Materials 393 (2009) 36–46

Contents lists available at ScienceDirect

Journal of Nuclear Materials

journal homepage: www.elsevier.com/locate/jnucmat

Tensile and fracture toughness properties of neutron-irradiated CuCrZr

Meimei Li *, M.A. Sokolov, S.J. Zinkle

Materials Science and Technology Division, Oak Ridge National Laboratory, Oak Ridge, TN 37831, USA

ARTICLE INFO

Article history:
Received 18 September 2008
Accepted 2 May 2009

ABSTRACT

Tensile and fracture toughness properties of a precipitation-hardened CuCrZr alloy were investigated in two heat treatment conditions: solutionized, water quenched and aged (CuCrZr SAA), and hot isostatic pressed, solutionized, slow-cooled and aged (CuCrZr SCA). The second heat treatment simulated the manufacturing cycle for large components, and is directly relevant for the ITER divertor components. Specimens were neutron irradiated at ~80 °C to two fluences, 2×10^{24} and 2×10^{25} n/m^2 ($E > 0.1$ MeV), corresponding to displacement doses of 0.15 and 1.5 displacements per atom (dpa). Tensile and fracture toughness tests were carried out at room temperature. Significant irradiation hardening and plastic instability at yield occurred in both heat treatment conditions with a saturation dose of ~0.1 dpa. Neutron irradiation slightly reduced fracture toughness in CuCrZr SAA and CuCrZr SCA. The fracture toughness of CuCrZr remained high up to 1.5 dpa ($J_Q > 200$ kJ/m^2) for both heat treatment conditions.

Published by Elsevier B.V.

1. Introduction

CuCrZr alloy is a prime candidate for high heat flux applications in the first wall and divertor components in the ITER burning plasma device currently under construction in France. CuCrZr is a precipitation-hardened alloy that exhibits high thermal conductivity, high strength, good ductility, radiation resistance, commercial availability, and low cost [1]. Heat treatments to achieve high strength of a precipitation-hardened alloy involve solution annealing at high temperature to dissolve alloying elements, water quenching to produce a super-saturated solid solution, and an aging treatment at an intermediate temperature to produce fine precipitates giving rise to high strength. Optimal combination of strength, ductility and thermal conductivity in CuCrZr can be reached by solution annealing at 980–1000 °C for 0.5–1 h, water quench, and aging at 450–500 °C for 2–4 h [2–4]. Slow cooling following the solution heat treatment or aging at high temperatures leads to coarsening of the fine precipitates and degradation of mechanical properties [5–8]. Therefore, the thermomechanical treatment experienced during alloy production, manufacturing cycle and in service can significantly affect the mechanical properties of CuCrZr.

During component manufacturing CuCrZr often experiences additional thermal cycles, such as brazing, welding, or hot isostatic pressing (HIPing). While solution annealing can be conducted during or after a brazing or HIPing process, rapidly quenching is not feasible for large components, and a much slower cooling rate (e.g. furnace cooled or gas cooled) is applied in the manufacturing cycle. Significant reduction in strength due to slow cooling rates has been reported in CuCrZr [5,6]. The effect of manufacturing cycles on physical and mechanical properties of CuCrZr is one of the main issues for its applications [9].

As reviewed elsewhere [10], neutron irradiation of copper and copper alloys at temperatures below ~250 °C produces substantial hardening and accompanying loss in tensile elongation. This phenomenon has historically been called low temperature 'radiation embrittlement', although there are relatively few actual measurements of fracture toughness following irradiation except for certain grades of steel. In both pure copper and a variety of copper alloys (as well as other materials), the 'embrittlement' is manifested by low values of uniform elongation due to localized necking (plastic instability). An open question is whether this reduced tensile ductility is an indicator of reduced fracture toughness.

The fracture toughness and the effect of neutron damage in CuCrZr are of great interest for ITER design and safety considerations. Only a limited amount of fracture toughness data on CuCrZr is available in the literature [11–18]. Large scatter in measured fracture toughness values was often observed due to different heat treatments, specimen geometry and dimensions, and testing methods. Fracture toughness data on the effect of neutron irradiation are available only up to a dose level of 0.3 dpa [16,17], whereas the anticipated exposure level for the CuCrZr components in ITER is ~1 dpa. Fracture toughness data at higher doses are needed to determine whether there is pronounced degradation for the ITER-relevant conditions. Neutron irradiation data of CuCrZr after ITER-relevant manufacturing cycles are also needed.

In this study, a CuCrZr alloy was examined in two heat-treated conditions, i.e. solution-annealed, quenched, and aged (referred to as 'CuCrZr SAA'), and HIP-treated, solutionized and slow-cooled,

* Corresponding author. Address: Nuclear Engineering Division, Argonne National Laboratory, 9700 South Cass Avenue, Argonne, IL 60439-4838, USA. Tel.: +1 630 2525111.
E-mail address: mli@anl.gov (M. Li).

0022-3115/$ - see front matter Published by Elsevier B.V.
doi:10.1016/j.jnucmat.2009.05.003

and aged (referred to as 'CuCrZr SCA'). The second heat treatment simulated the manufacturing cycle for large components, and is directly relevant for the ITER divertor components. Irradiation experiments were performed at reactor ambient temperature (~80 °C) to two fluences of 2×10^{24} and 2×10^{25} n/m^2 ($E > 0.1$ MeV) (~0.15 and 1.5 dpa) to examine the effect of heat treatment and neutron irradiation on tensile and fracture toughness properties of the alloy. This study examined the effect of neutron irradiation on the fracture toughness data of CuCrZr up to 1.5 dpa, which exceeds the ITER design dose for divertor structural components.

2. Experimental procedure

CuCrZr was manufactured according to the specifications for Elbrodur® G grade, and was provided by KM Europa Metal AG. The chemical composition was 98.97 wt% Cu–0.84 wt% Cr–0.14 wt% Zr. The as-received material was in a plate form with a thickness of 30 mm in the ITER solution-annealed and aged condition (CuCrZr SAA) (solution annealing at 980–1000 °C for 30–60 min, water quench and age at 460–500 °C for 2–4 h). The as-received material was further HIP-treated at 1040 °C for 2 h at 140 MPa followed by solutionizing at 980 °C for 0.5 h with a slow cooling rate of 50–80 °C/min between 980 and 500 °C, and final aging at 560 °C for 2 h (CuCrZr SCA). Optical micrographs of unirradiated CuCrZr SAA and CuCrZr SCA are shown in Fig. 1. The average grain size was ~27 μm for CuCrZr SAA, and >500 μm for CuCrZr SCA.

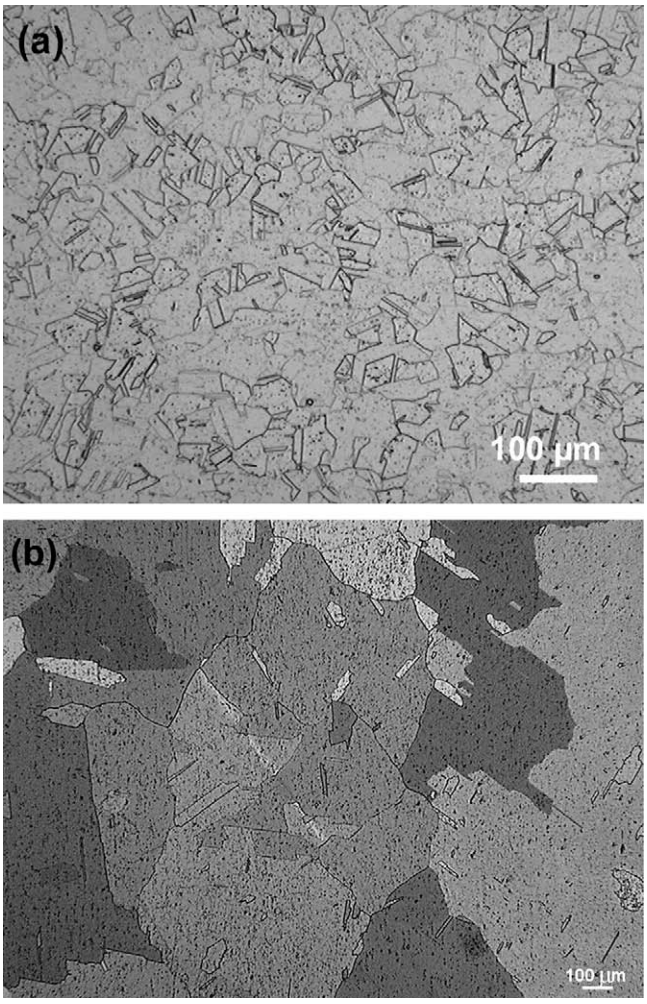

Fig. 1. Optical micrographs of unirradiated (a) CuCrZr SAA and (b) CuCrZr SCA.

The microstructure of unirradiated CuCrZr SAA and CuCrZr SCA was examined in a FEI Tecnai20 transmission electron microscope (TEM) operating at 200 kV. The 3 mm TEM disc specimens were electropolished in a Tenupol twin-jet polishing unit using a solution of 1000 ml methanol, 60 ml nitric acid, and 10 ml 2-butoxyethanl cooled to −50 °C at 50 V. TEM examination was performed using combined bright field and weak beam dark field (WBDF) imaging techniques. Weak beam dark field (WBDF) imaging conditions were at $g(5g)$, $g = 002$ near the zone axis of $[\bar{1}\ 1\ 0]$. Precipitate size and number density were determined using WBDF images.

Type SS-3 sheet tensile specimens were machined with the gauge parallel to the rolling direction from the CuCrZr SAA and the CuCrZr SCA plates to examine the effect of neutron irradiation on tensile properties. The type SS-3 tensile specimens had gauge dimensions of $7.62 \times 1.52 \times 0.50$ mm with a total length of 25.4 mm. A schematic drawing of the type SS-3 tensile specimen is given in Fig. 2. Single edge-notched bend (SE(B)) specimens loaded in three-point bending were used for fracture toughness tests. The selection of geometry and dimensions of fracture toughness specimens was dictated by the size limitations imposed by the hydraulic rabbit capsules in the target region of the High Flux Isotope Reactor (HFIR). A perforated rabbit capsule has an internal diameter of 10 mm and an internal length of 53 mm, which led to the selection of a SE(B) specimen with dimensions of $40 \times 8 \times 4$ mm. The SE(B) specimen had a starter notch of 2 mm and was oriented in the T-L orientation (crack growth in the rolling direction). A schematic drawing of the SE(B) specimen is shown in Fig. 3. Due to small specimen sizes and highly ductile nature of the alloy there was a concern whether the SE(B) specimens would provide useful data, particularly for the unirradiated CuCrZr, as the irradiation was expected to result in higher strength and lower toughness. Therefore, 0.18T disk compact tension (DCT) specimens, which gave valid fracture toughness results of the same alloy in a previous study [18], were also used for fracture toughness measurements in the unirradiated condition. The 0.18T DCT specimens have a diameter of 12.5 mm and a thickness of 4.62 mm, which is too large to be accommodated in the HFIR hydraulic rabbit tube capsule. A schematic drawing of the 0.18T DCT specimens is given in Fig. 4. The DCT specimens were machined in the T-L orientation from the same plates as those used for SE(B) specimens. All SE(B) and 0.18T DCT specimens were fatigue precracked before testing or neutron irradiation following the ASTM Standard E1820-06 'Standard Test Method for Measurement of Fracture Toughness' [19]. Fatigue precracking was carried out on a 44-kN (10,000 lbf) servohydraulic test machine with a frequency of 30 Hz in the stroke mode at room temperature in air. After fatigue precracking, all specimens were side grooved to 20% of their thickness with 10% on each side.

Irradiation of the SE(B) and SS-3 tensile specimens was conducted in the HFIR hydraulic tube facility. Eight perforated rabbit capsules were constructed and irradiated, with each capsule containing one SE(B) specimen and one or two SS-3 tensile specimen(s). Perforated rabbit capsules allow specimens in direct contact with the flowing water to maintain the specimen temperature at the reactor coolant temperature. Due to concerns of local pitting corrosion of the aluminum clad of HFIR fuel elements by copper ions in aqueous solution, double protection was required for each SE(B) and SS-3 specimen. Specimens were plated with high-purity Al to a minimum thickness of 12.5 μm by AlumiPlate Inc. All Al-plated specimens were inspected under a microscope, and the complete coverage of all copper specimen surfaces of the plated layer with minimum plating thickness of 12.5 μm were confirmed. The aluminum plating was also examined metallographically at ORNL. The metallographic samples were taken from a

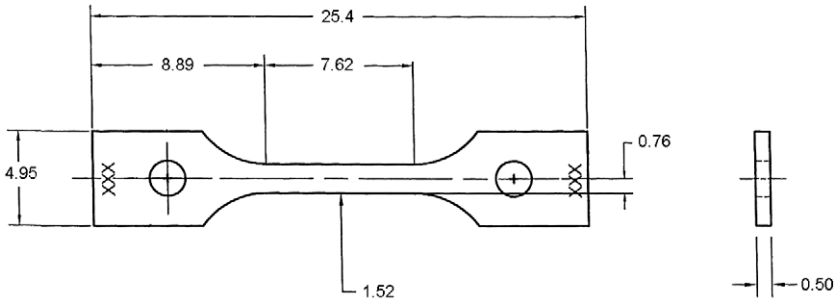

Fig. 2. Schematic drawing of a type SS-3 sheet tensile specimen (unit: mm).

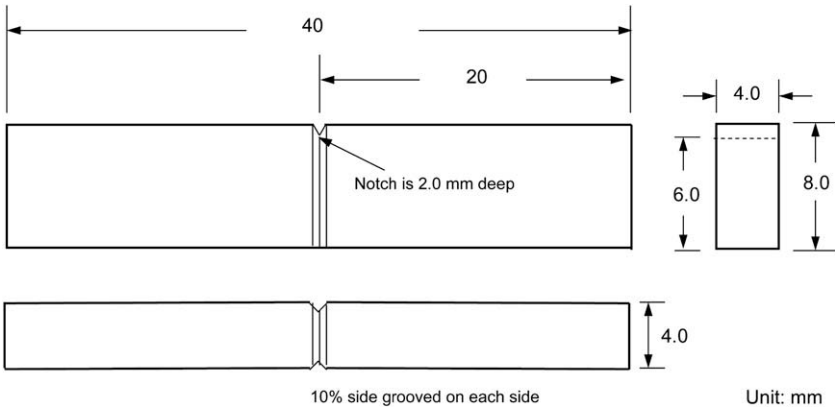

Fig. 3. Schematic drawing of a SE(B) specimen.

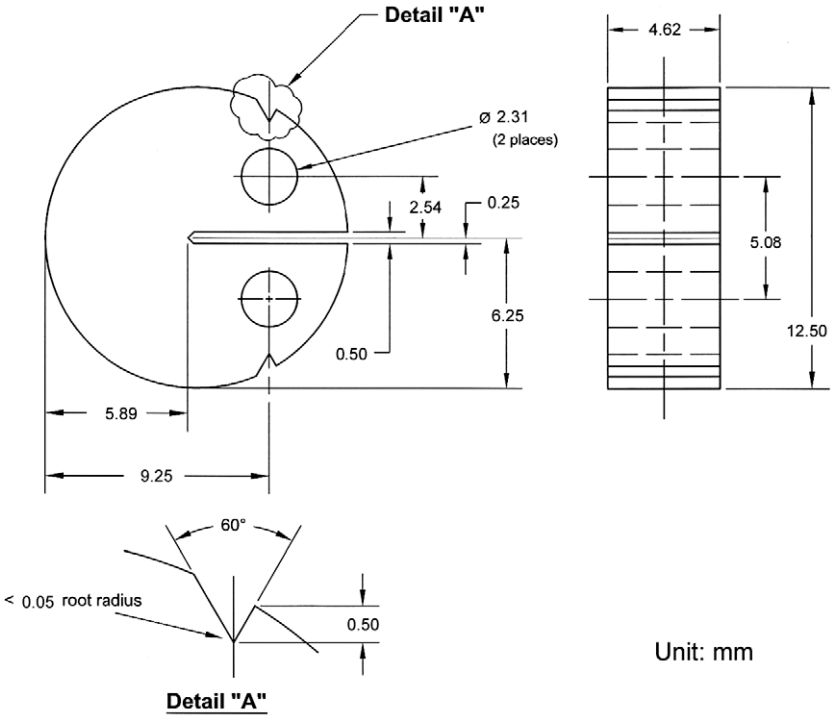

Fig. 4. Schematic drawing of a 0.18T disk compact tension (DCT) specimen.

few random locations of a bend bar specimen including the area around a notch. The micrographs of aluminum coating showed that the quality of the plating was excellent with good adhesion to the substrate, uniform thickness, and no evidence of porosity or cracks. As an additional safeguard, each Al-coated specimen was sealed individually in an envelope of 75 μm Al foil by electron beam

Table 1
Neutron irradiation conditions.

Capsule ID	Heat treatment	Specimen type	Irradiation temperature (°C)	Fluence ($E > 0.1$ MeV) (n/m^2)	Dose (dpa)
CZ1	SCA	SE(B), SS-3	80	2.08×10^{25}	1.5
CZ2	SCA	SE(B), SS-3	80	2.08×10^{25}	1.5
CZ3	SAA	SE(B), SS-3	80	2.08×10^{25}	1.5
CZ4	SAA	SE(B), SS-3	80	2.08×10^{25}	1.5
CZ5	SCA	SE(B), SS-3	80	1.97×10^{24}	0.14
CZ6	SCA	SE(B), SS-3	80	2.01×10^{24}	0.15
CZ7	SAA	SE(B), SS-3	80	1.94×10^{24}	0.14
CZ8	SAA	SE(B), SS-3	80	1.97×10^{24}	0.14

welding in vacuum. Upon exposure to air after welding, the atmospheric pressure compresses the foil tightly around the specimen. The tight contact between the Al foil and the specimen ensured that the irradiation temperature of the specimen was close to the reactor coolant temperature, ~80 °C. The Al foil was removed following irradiation, prior to mechanical property testing.

Four of the eight rabbit capsules experienced irradiation to a nominal neutron fluence of $\sim 2.0 \times 10^{24}$ n/m^2 ($E > 0.1$ MeV), corresponding to a damage level of ~0.15 dpa; the other four rabbit capsules were irradiated to a nominal neutron fluence of $\sim 2.0 \times 10^{25}$ n/m^2 ($E > 0.1$ MeV), ~1.5 dpa. This ensured that duplicate irradiation tests could be performed on CuCrZr SAA and CuCrZr SCA specimens at each neutron dose. The irradiation conditions are summarized in Table 1.

Tensile tests were performed on a MTS screw-driven machine at room temperature in air at strain rates of 0.001 and 0.1 s^{-1}. The engineering tensile properties were determined from an analysis of the load vs. cross-head displacement electronic data files. Fracture toughness tests were conducted in accordance with the ASTM Standard E 1820-06 'Standard Test Method for Measurement of Fracture Toughness' using a computer-controlled test and data acquisition system [19,20]. All the tests were performed at room temperature in air. The unirradiated SE(B) specimens were tested with a linear variable displacement transducer (LVDT), and the unirradiated DCT specimens were tested with an outboard clip gage on a 222-kN (50,000 lbf) servohydraulic test machine. Irradiated SE(B) specimens were tested in a hot cell facility on a similar 490-kN (110,000 lbf) servohydraulic test machine in the stroke mode. To minimize effects of the electroplated Al coating on the fatigue precrack, a few fatigue cycles with the final maximum and minimum loads used for fatigue precracking were applied to the specimens prior to the J–R testing. Crack growth was monitored by the unloading compliance technique. The unloading compliance method used for calculating the J-integral is described in the Ref. [21]. After testing, the specimens were heat tinted by placing them on a hot plate and heating them until a noticeable color change occurred. The specimens were cooled to room temperature and then broken open to allow measurement of initial and final crack lengths. The crack lengths were calculated by the nine-point average method. Fracture surface of unirradiated specimens were examined by scanning electron microscopy (SEM).

3. Experimental results

3.1. Microstructure of unirradiated CuCrZr SAA and CuCrZr SCA

Representative weak beam dark field images of precipitate microstructure for unirradiated CuCrZr SAA and CuCrZr SCA are shown in Fig. 5. Precipitates in CuCrZr SAA were small Guinier–Preston (G–P) zones, uniformly distributed in the matrix showing primarily black dot types and a small number of precipitates with lobe–lobe contrast. The number density of precipitates in CuCrZr SAA was $\sim 4.3 \times 10^{22}$/m^3, and the mean diameter was ~3 nm, which is comparable with previous findings [22–24]. Compared with CuCrZr SAA, CuCrZr SCA had a lower number density of larger precipitates with a mixture of coherent and incoherent particles. The number density of precipitates in CuCrZr SCA was $\sim 1.9 \times 10^{22}$/m^3, and the mean diameter ~9 nm. The nature of these small precipitates was not determined. Previous work suggested that they are primarily Cr-rich precipitates with either body centered cubic (bcc) or face centered cubic (fcc) structure [22–25]. In both CuCrZr SAA and CuCrZr SCA, there was a very low number density of large particles in the grain interior. Precipitate free zones at grain boundaries were also observed.

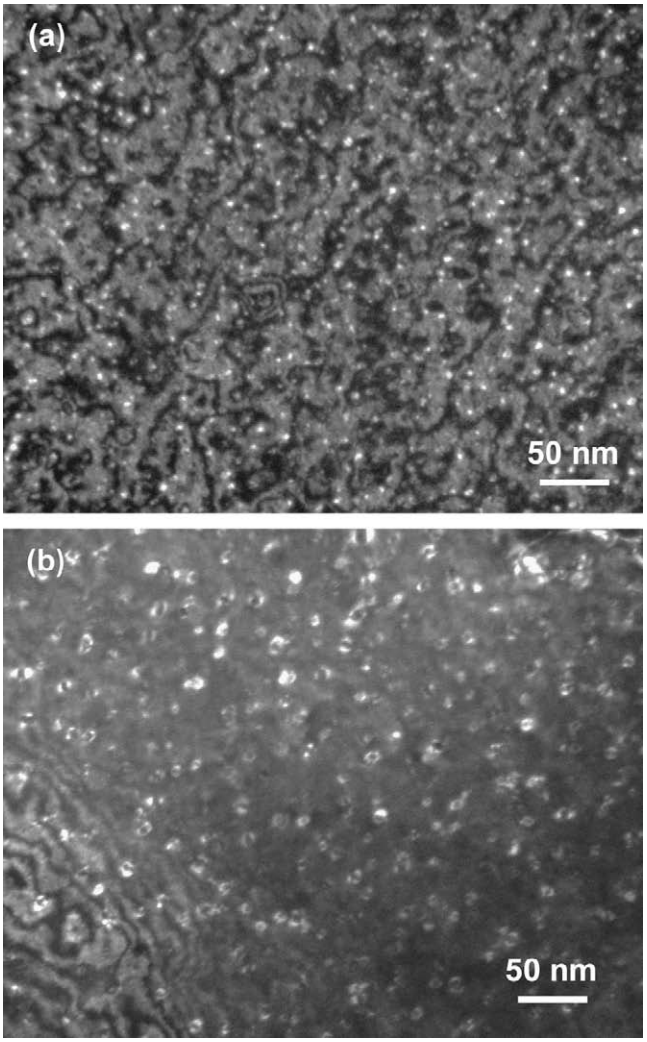

Fig. 5. Representative weak beam dark field images showing precipitates in unirradiated (a) CuCrZr SAA and (b) CuCrZr SCA.

3.2. Tensile properties

A summary of all of the measured tensile data i.e. yield stress (YS), ultimate tensile strength (UTS), uniform elongation (UE) and total elongation (TE) is given in Table 2. The yield stress was measured at the 0.2% offset when macroscopic strain hardening occurred or at the maximum stress if no macroscopic strain hardening (i.e. prompt necking with UE < 0.2%) was observed. All the tensile data on unirradiated and irradiated CuCrZr SAA and CuCrZr SCA were measured on Al-coated SS-3 tensile specimens. The tensile data were not corrected for the influence of the Al coat-

Table 2
Tensile properties of unirradiated and irradiated CuCrZr SAA and CuCrZr SCA.

Heat Treat	Capsule ID	Dose (dpa)	Strain rate (1/s)	YS (MPa)	UTS (MPa)	UE (%)	TE (%)
SCA	–	0	0.001	204	298	13	17
SCA	–	0	0.001	216	299	11	16
SCA	CZ5	0.14	0.001	367	367	0.1	8
SCA	CZ5	0.14	0.001	394	394	0.2	14
SCA	CZ6	0.15	0.001	405	405	0.2	6
SCA	CZ1	1.5	0.001	363	370	2	9
SCA	CZ2	1.5	0.001	363	371	5	12
SCA	–	0	0.1	223	316	8	13
SCA	CZ1	1.5	0.1	386	386	0.5	8
SCA	CZ2	1.5	0.1	388	388	0.4	15
SAA	–	0	0.001	311	441	21	32
SAA	CZ7	0.14	0.001	532	532	0.2	7
SAA	CZ8	0.14	0.001	536	536	0.1	7
SAA	CZ3	1.5	0.001	473	473	0.3	12
SAA	CZ4	1.5	0.001	484	484	0.1	10
SAA	–	0	0.1	308	444	19	27
SAA	CZ7	0.14	0.1	561	561	0.7	8
SAA	CZ3	1.5	0.1	518	518	0.5	12
SAA	CZ4	1.5	0.1	528	528	0.7	13

ing. The specimen dimensions used for tensile property calculations were the SS-3 true dimensions before coating. Assuming an Al plating thickness of 12.5–17 μm (corresponding to an Al coating thickness 5–7% of the Cu alloy thickness), and using the reported strengths of unirradiated and irradiated Al [26], the contribution from the Al coating is calculated to be <3 MPa and <8 MPa for unirradiated and 1.5 dpa conditions, respectively.

The engineering stress–strain curves of SS-3 tensile specimens tested at room temperature at a strain rate of 0.001 s^{-1} are shown in Fig. 6 for the CuCrZr SAA and CuCrZr SCA before and after neutron irradiation. The unirradiated CuCrZr SAA specimens exhibited a yield stress 311 MPa and a uniform elongation 21%. The yield stress of CuCrZr SAA increased significantly after irradiation to 0.14 dpa, accompanied by early onset of necking at the yield point. The total elongation after irradiation to 0.14 dpa was reduced to about one-fourth of the unirradiated value. Compared to the 0.14 dpa specimens, the yield stress decreased and the total elongation somewhat increased upon further irradiation to 1.5 dpa.

The yield stress of unirradiated CuCrZr SCA was significantly lower (~100 MPa lower) than the yield stress of unirradiated CuCrZr SAA. The uniform and total elongations measured for unirradiated CuCrZr SCA were also significantly less than those for the SAA condition. Neutron irradiation to 0.15 dpa resulted in a significant increase in yield stress and a complete loss of macroscopic strain hardening capacity and plastic instability at the yield point, qualitatively similar to the behavior observed for the irradiated CuCrZr SAA specimens. A significant scatter of stress–strain response was observed for the CuCrZr SCA at this dose level, even for specimens in the same irradiation capsule. Further irradiation to 1.5 dpa produced flow localization behavior qualitatively similar to the 0.15 dpa CuCrZr SCA specimens, and the change in strength was insignificant compared to the 0.15 dpa specimens.

The dose dependence of tensile properties is shown in Fig. 7 for CuCrZr SAA and CuCrZr SCA. Previously reported data for solution-annealed and aged CuCrZr from the ITER Materials Property Handbook (MPH) [2] are included in Fig. 7. Only the tensile data at irradiation temperatures of 60–100 °C and at test temperatures near irradiation temperatures were considered. The large variation of tensile stresses for unirradiated CuCrZr is most likely due to its sensitivity to heat treatment [1,3,4]. The yield stress and UTS of unirradiated CuCrZr SAA fall in the scatter band of the ITER MPH data, while the values of yield stress and UTS for irradiated CuCrZr SAA are higher than what were reported in the ITER MPH. The tensile stress data for both unirradiated and irradiated CuCrZr SCA are

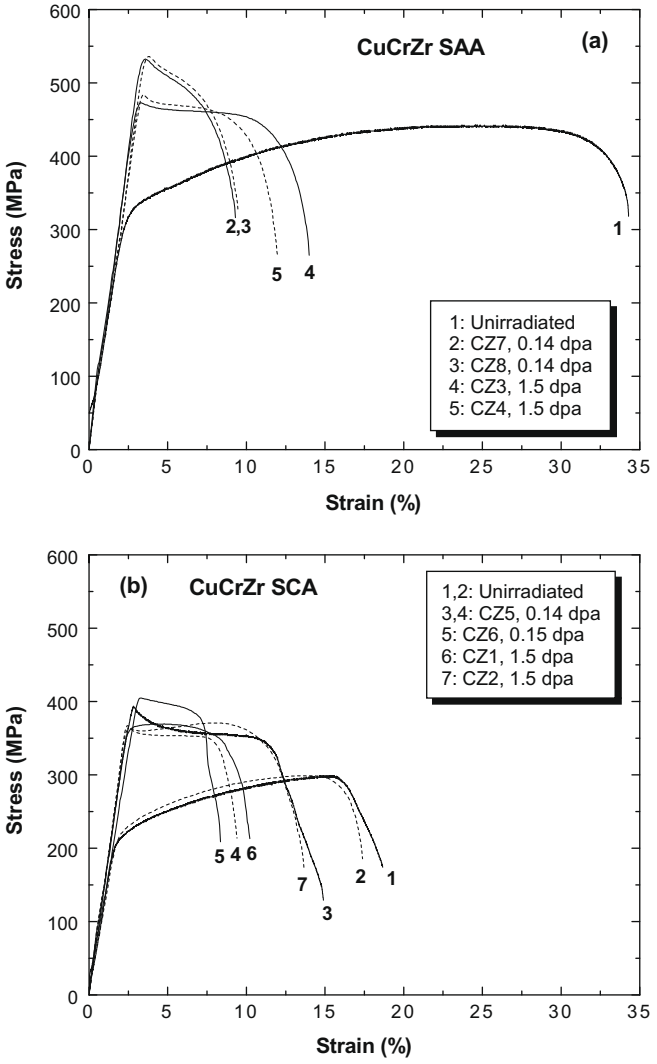

Fig. 6. Engineering stress–strain curves of (a) the CuCrZr SAA and (b) the CuCrZr SCA tested at room temperature and a strain rate of 0.001 s^{-1}.

lower than the minimum CuCrZr SAA values given in the ITER MPH. Significant variations in uniform and total elongations were observed in CuCrZr, although in all cases there was a decrease in elongation with increasing dose up to ~0.1 dpa. The ductility data of CuCrZr SAA and CuCrZr SCA match well with the ITER MPH results, except that the 1.5 dpa specimens showed higher total elongations than those reported in the ITER MPH.

The effect of neutron irradiation on tensile properties was quite similar in CuCrZr SAA and CuCrZr SCA. Significant irradiation hardening is clearly demonstrated in both CuCrZr SAA and CuCrZr SCA in Fig. 7(a). The saturation of hardening occurred at ~0.1 dpa with an average hardening increment of ~200 MPa. Further irradiation to 1.5 dpa decreased the yield stress. The ultimate tensile strength of irradiated CuCrZr was less sensitive to neutron dose than the yield stress. Plastic instability at yield and complete loss of uniform elongation occurred at ~0.1 dpa, while the alloy still retained sufficient ductility with the minimum value of total elongation above ~5% (see Fig. 7(c) and (d)).

CuCrZr SAA and CuCrZr SCA were tested at two different strain rates to examine the strain-rate dependence of tensile properties. Representative engineering stress–strain curves for unirradiated and irradiated CuCrZr SAA and CuCrZr SCA are shown in Fig. 8, and the strain rate dependence of the yield stress are shown in Fig. 9. Tensile data of unirradiated CuCrZr in the ITER solution-

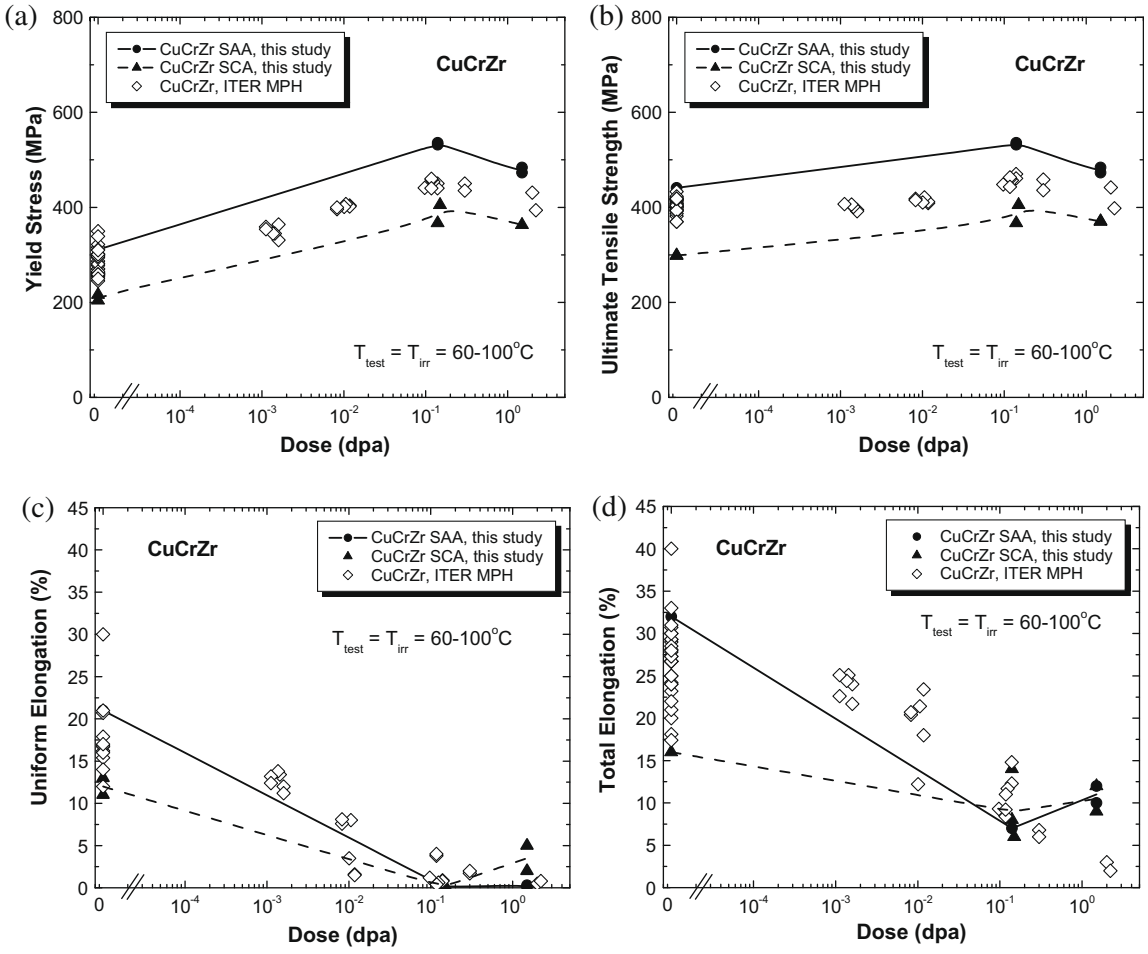

Fig. 7. Dose dependence of (a) yield stress, (b) ultimate tensile strength, (c) uniform elongation, and (d) total elongation for CuCrZr SAA and CuCrZr SCA.

annealed and aged treatment reported by Zinkle et al. [27] were included for comparison. The yield stresses for unirradiated CuCrZr SAA and CuCrZr SCA were relatively insensitive to the strain rate. Neutron irradiation introduced significant hardening in the two alloy conditions, while the dependence of the yield stress on the strain rate was only slightly affected by neutron irradiation. A small increase in strain-rate dependence of the yield stress was observed in both CuCrZr SAA and CuCrZr SCA with a higher yield stress at a higher strain rate. The increase in strain-rate dependence was somewhat higher in CuCrZr SAA than in CuCrZr SCA. Early onset of necking and loss of uniform elongation occurred in all irradiated specimens tested at a strain rate of 0.1 s^{-1}.

3.3. Fracture toughness

The fracture toughness of unirradiated CuCrZr SAA and CuCrZr SCA was determined by testing two DCT specimens and two SE(B) specimens for each heat treatment condition. Eight SE(B) specimens, four each of CuCrZr SAA and CuCrZr SCA, were tested after neutron irradiation to two nominal doses of 0.15 and 1.5 dpa. All SE(B) and DCT specimens were tested to a load line displacement limit without failure. Significant plasticity was observed. No crack extension occurred in any unirradiated SE(B) specimens, while all four DCT specimens showed a small amount of stable crack growth. Three of the four irradiated SE(B) CuCrZr SAA specimens showed some crack extension, while crack extension was observed only on one irradiated SE(B) CuCrZr SCA specimen. Note that the yield and tensile strength of irradiated CuCrZr SAA were considerably higher than that of irradiated CuCrZr SCA. For the tests that did not show any crack extension, the maximum *J-value* was reported, and in this case, $J_{max} < J_Q$ (an example is given in Fig. 10). For the specimens exhibiting some crack extension, there were insufficient data points in the stable crack growth stage to determine J_Q accurately. The J_Q values were estimated from the *J–R* curves by the intersection of the regression line with the 0.2-mm offset line (an example is given in Fig. 11).

The fracture toughness data of CuCrZr SAA and CuCrZr SCA are summarized in Table 3. The data of the J_Q (or J_{max}) value are plotted as a function of dose in Fig. 12. The J_Q values of unirradiated CuCrZr SAA and CuCrZr SCA are quite similar (~330–400 kJ/m^2). Neutron irradiation slightly reduced the J_Q value for both CuCrZr SAA and CuCrZr SCA, though the J_Q values remain appreciably high up to 1.5 dpa, with J_Q values >200 kJ/m^2 (equivalent to $K_Q \sim 170$ MPa$\sqrt{m}$).

Compared with the fracture toughness data for solution annealed and aged CuCrZr in the ITER MPH [2] (see Fig. 12), the fracture toughness data for CuCrZr SAA and SCA in the unirradiated and irradiated to ~0.15 dpa conditions fall within the data scatter band. The large scatter in the measured fracture toughness values are possibly due to poorly defined heat treatments, specimen geometry and dimensions, and test techniques [2]. In particular, it should be noted that the validation criteria in the ASTM standards were not satisfied in most of experiments as a result of high ductility of the alloy. The current study extends fracture toughness

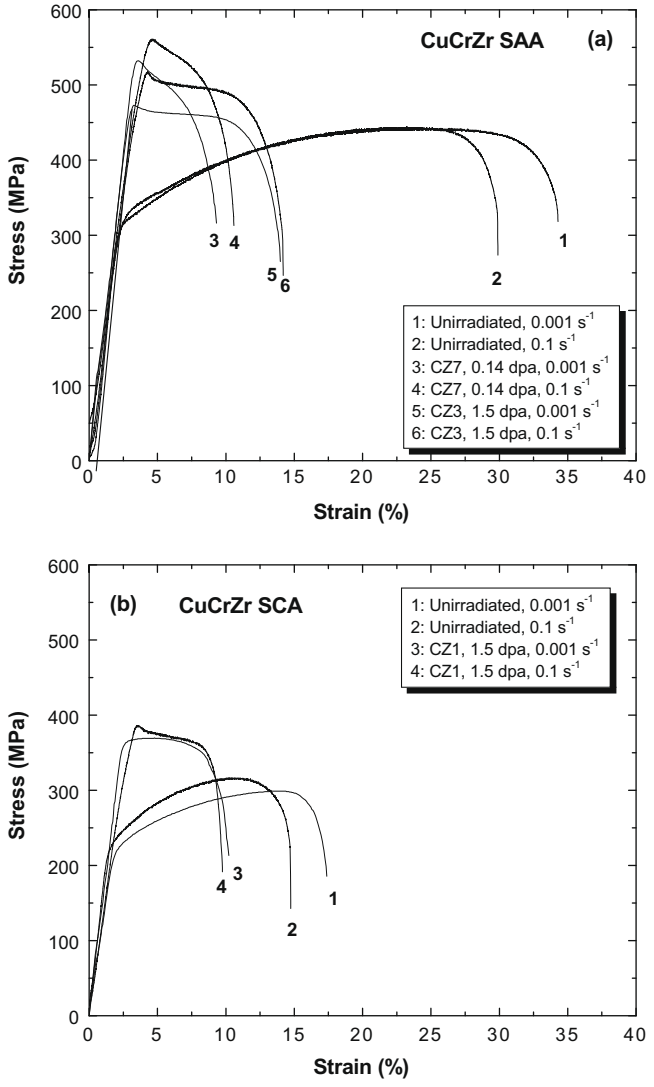

Fig. 8. Engineering stress–strain curves for (a) the CuCrZr SAA and (b) the CuCrZr SCA tested at two different strain rates at room temperature.

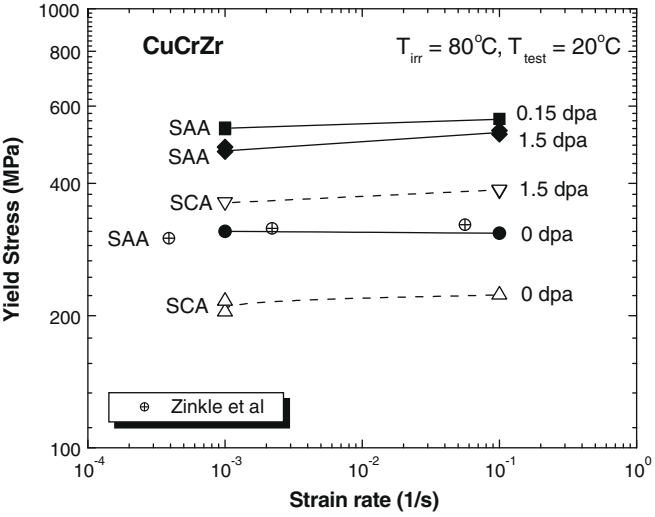

Fig. 9. Strain rate dependence of the yield stress in unirradiated and irradiated CuCrZr SAA and CuCrZr SCA.

data of neutron-irradiated CuCrZr to 1.5 dpa. For all investigated doses and heat treatment conditions up to 1.5 dpa, high fracture toughness is observed with only a slight reduction due to neutron exposure, in contrast to the marked decrease in uniform and total elongations.

Fracture surfaces of unirradiated and irradiated SE(B) and DCT specimens were examined by SEM. Representative SEM images of a SE(B) and DCT specimen for unirradiated CuCrZr SAA and a SE(B) specimen for unirradiated CuCrZr SCA are shown in Fig. 13. The regions of fatigue-precracking and final fracture are labeled, and the region of stable crack extension is marked by a rectangular box. SEM images confirmed the extent of stable crack growth shown in the *J*–*R* curves. For example, the CuCrZr SAA DCT specimen C17 showed significant crack extension and the CuCrZr SCA SE(B) specimen MB02 showed no crack extension under SEM, which are consistent with the *J*–*R* curve calculations. The DCT specimen (C17) showed more significant stable crack extension than the SE(B) specimen (C02) for CuCrZr SAA.

Representative SEM images of irradiated SE(B) specimens are given in Fig. 14 for CuCrZr SAA and CuCrZr SCA irradiated to 0.14–0.15 dpa. Both the SAA-0.14 dpa specimen (C07) and the SCA-0.15 dpa specimen (MB03) showed stable crack growth, as seen in the *J*–*R* curves. It is noted that the SCA-0.15 dpa specimen (MB01) showed an unbroken ligament area between two crack extension regions.

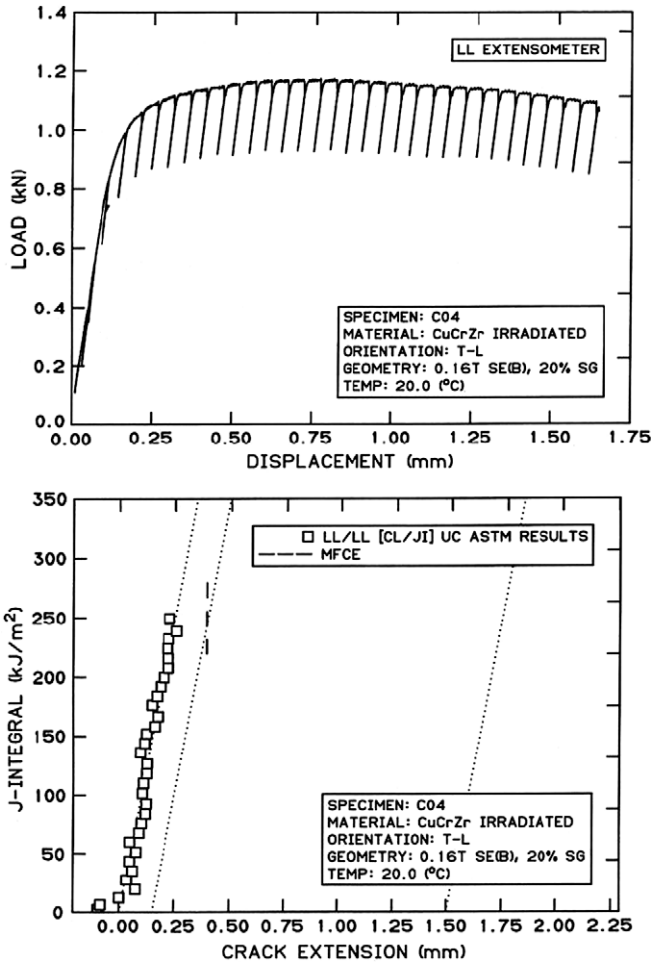

Fig. 10. An example showing the determination of the fracture toughness for a test that did not show any crack extension. The maximum *J*-value was reported, and in this case, $J_{max} < J_Q$.

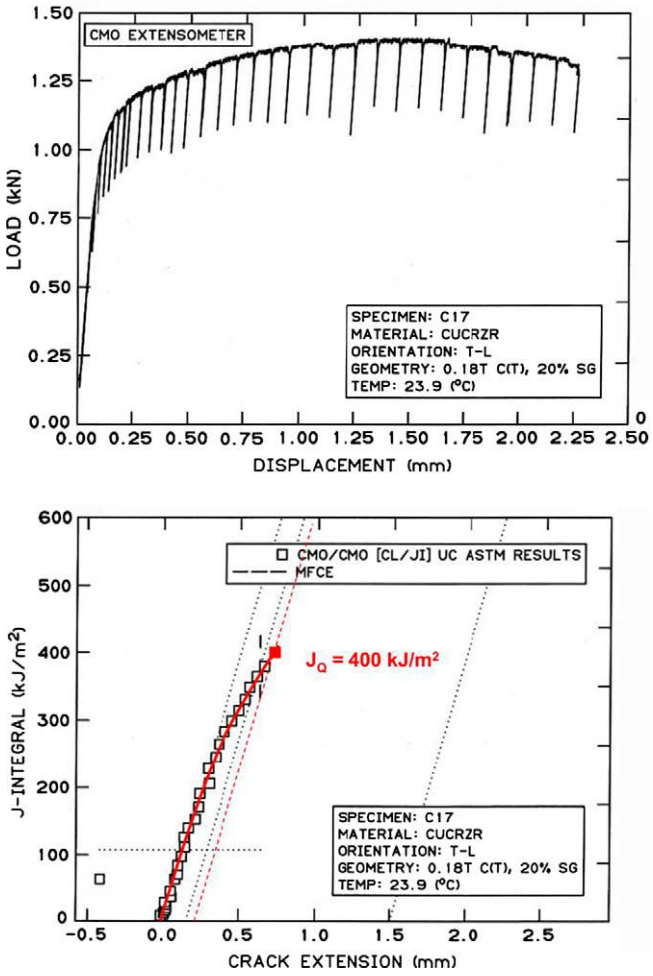

Fig. 11. An example showing the determination of the fracture toughness for a test exhibiting some crack extension. The J_Q values were estimated from the *J–R* curves by the intersection of the regression line with the 0.2-mm offset line.

4. Discussion

4.1. Effect of heat treatment on mechanical properties

The effect of manufacturing cycles on mechanical properties was investigated by comparing tensile behavior and fracture toughness of CuCrZr SAA and CuCrZr SCA with the thermomechanical treatment simulating the manufacturing cycle for large components. It is shown that the slow cooling rate (50–80 °C/min) and overaging at 560 °C/2 h significantly reduced the yield stress and the ultimate tensile strength, and tensile elongations of CuCrZr SCA relative to CuCrZr SAA. Previous studies have found that cooling rates >1200 °C/min are required to fully quench the Cu–Cr solid solution [28–30]. The relatively slow cooling rate in the CuCrZr SCA treatment resulted in a lower nucleation rate (due to reduced Cr supersaturation levels) and more rapid precipitate coarsening compared to the optimum CuCrZr SAA treatment. Overaging can also lead to precipitate coarsening. The SCA treatment also resulted in a significant larger grain size compared to the SAA condition. It is noted that the average grain size of CuCrZr SCA is comparable to the gauge thickness of the tensile specimens. The large grain size and very few grains across the tensile gauge thickness in the CuCrZr SCA specimens may lead to larger variability of tensile strength data, and a reduction in measured tensile elongation. Previous studies evaluated by Jung et al. [31] have found that a minimum of 4–6 grains are usually needed to obtain bulk tensile properties.

The effect of heat treatment on fracture toughness of CuCrZr was much less pronounced than its effect on tensile properties. CuCrZr SCA has somewhat lower fracture toughness than that of CuCrZr SAA.

Table 3
Fracture toughness of unirradiated and irradiated CuCrZr SAA and CuCrZr SCA.

Capsule ID	Heat	Orient	Spec type	T_{irr} (°C)	Dose (dpa)	T_{test} (°C)	J_{max} (<J_Q) (kJ/m^2)	J_Q (kJ/m^2)
–	SCA	T-L	DCT	–	0	22		344
–	SCA	T-L	DCT	–	0	22		350
–	SCA	T-L	SE(B)	–	0	22	202	N/A
–	SCA	T-L	SE(B)	–	0	22	207	N/A
CZ5	SCA	T-L	SE(B)	80	0.14	22	251	N/A
CZ6	SCA	T-L	SE(B)	80	0.15	22		248
CZ1	SCA	T-L	SE(B)	80	1.5	22	234	N/A
CZ2	SCA	T-L	SE(B)	80	1.5	22	323	N/A
–	SAA	T-L	DCT	–	0	22		400
–	SAA	T-L	DCT	–	0	22		333
–	SAA	T-L	SE(B)	–	0	22	195	N/A
–	SAA	T-L	SE(B)	–	0	22	233	N/A
CZ7	SAA	T-L	SE(B)	80	0.14	22		290
CZ8	SAA	T-L	SE(B)	80	0.14	22		353
CZ3	SAA	T-L	SE(B)	80	1.5	22	249	N/A
CZ4	SAA	T-L	SE(B)	80	1.5	22		265

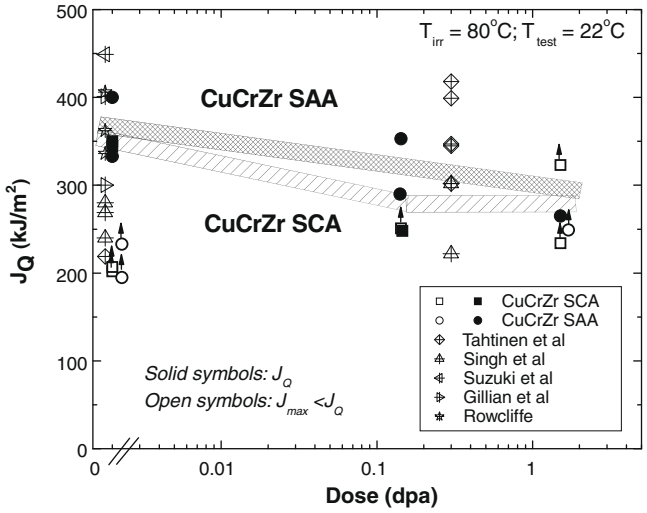

Fig. 12. Fracture toughness of CuCrZr SAA and CuCrZr SCA as a function of dose. Comparison of fracture toughness data obtained in this study with those included in the ITER MPH is also shown.

4.2. Effect of neutron irradiation on mechanical properties

The tensile behavior of irradiated CuCrZr SAA and CuCrZr SCA is quite similar, as seen in Figs. 6 and 7. Significant irradiation hardening occurred in both alloy conditions irradiated to 0.14–0.15 dpa. The similarity in hardening implies that the formation and accumulation of defects and defect clusters is the main contributor to hardening, and that the differences in precipitate sink strength for the two heat treatment conditions does not have a pronounced effect on their irradiated behavior.

For both heat treatments, the significant hardening in irradiated CuCrZr is accompanied by complete loss of macroscopic strain hardening capability and plastic instability at yield. In a few cases, the yield drop in irradiated CuCrZr SAA was more pronounced than in CuCrZr SCA irradiated to 0.14–0.15 dpa. Edwards et al. [7,32] studied the role of over-aged precipitates in inhibiting plastic flow localization in neutron-irradiated CuCrZr, and found that the lower

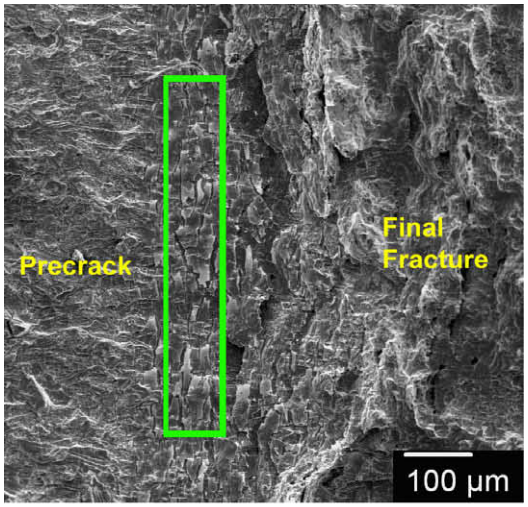

(a) SE(B) specimen C02 – CuCrZr SAA.

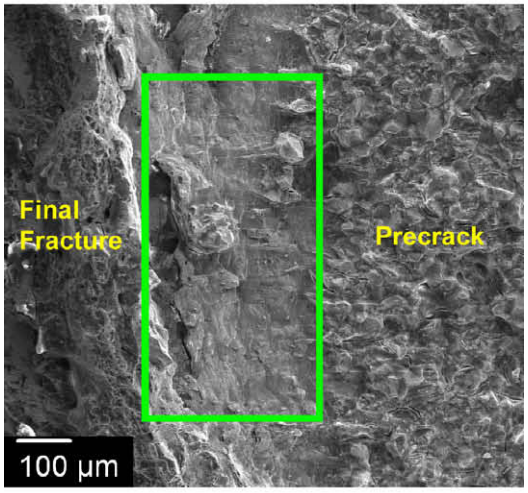

(b) DCT specimen C17 – CuCrZr SAA.

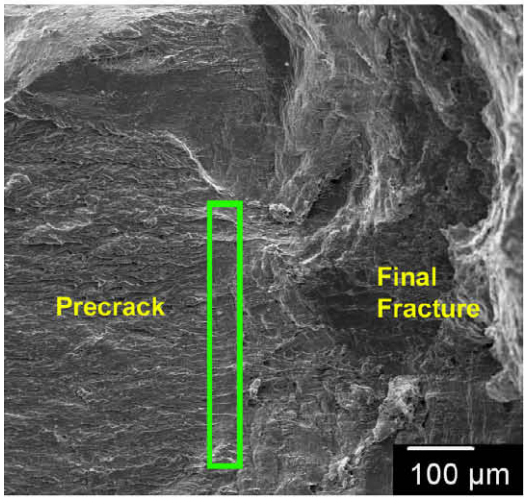

(c) SE(B) specimen MB02 – CuCrZr SCA.

Fig. 13. SEM fractography of unirradiated SE(B) specimens and DCT specimens for CuCrZr SAA and CuCrZr SCA.

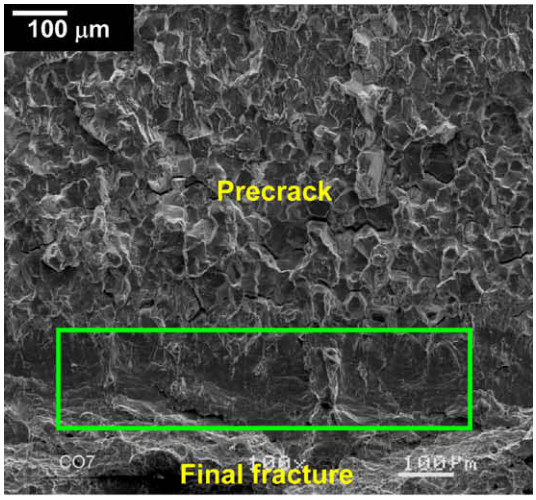

(a) SE(B) specimen C07 – CuCrZr SAA (0.14 dpa)

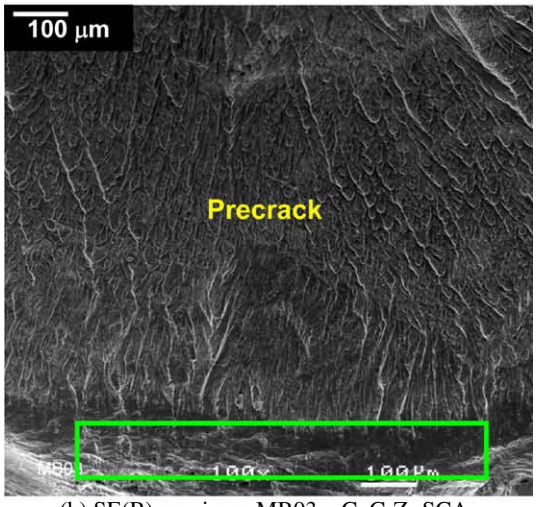

(b) SE(B) specimen MB03 – CuCrZr SCA (0.15 dpa)

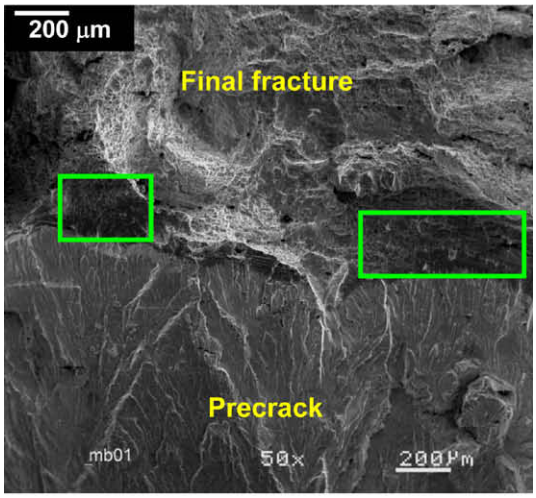

(c) SE(B) specimen MB01 – CuCrZr SCA (0.14dpa)

Fig. 14. SEM fractography of irradiated SE(B) specimens for CuCrZr SAA and CuCrZr SCA.

density of large particles in over-aged CuCrZr improved resistance to plastic instability. The rational was that the precipitates in the prime-aged CuCrZr were too small to effectively prevent localized deformation and dislocation channeling that occurred after neutron irradiation. The less pronounced yield drop in CuCrZr SCA may be attributed to over-aged precipitate particles. Though some

improvement of resistance in localized flow and yield drop occurred in overaged CuCrZr, dislocation channeling was observed by Edwards in both prime-aged and over-aged CuCrZr following irradiation [7,32]. Detailed analysis of as-irradiated and as-irradiated and deformed microstructure of CuCrZr SAA and SCA is necessary to fully understand the radiation damage and its effect on deformation behavior.

It was found that the values of yield stress and UTS for irradiated CuCrZr SAA are higher than what were reported in the ITER MPH, while the yield stress and UTS of unirradiated CuCrZr SAA fall in the scatter band of the ITER MPH data (see Fig. 7). Cooling rate during quenching is normally not well defined and therefore subsequent aging heat treatments can result in relatively large variations in tensile strength of CuCrZr alloy. Fig. 7 indicates that some of the irradiated CuCrZr alloy in the ITER MPH may have experienced a slower cooling rate than the reported rapid water-quenching. It may also be possible that the relatively high rate of solute transmutation production in copper irradiated in the HFIR (due to the high thermal neutron flux relative to the fast neutron flux) lead to an enhancement in overall strengthening in the CuCrZr following HFIR neutron irradiation compared to some of the other studies in the ITER database.

Despite that both CuCrZr SAA and CuCrZr SCA showed significant irradiation hardening as well as complete loss of strain hardening capability and flow localization even after low-dose irradiation (0.14–0.15 dpa), the effect of neutron irradiation on fracture toughness of CuCrZr was less pronounced. Reduction of fracture toughness in irradiated CuCrZr SAA and CuCrZr SCA was small, and the J_Q value was still >200 kJ/m^2 up to 1.5 dpa. The *J–R* curves indicated that only some of the SE(B) specimens showed small amounts of stable crack extension (mostly in CuCrZr SCA), while some did not show any crack extension (mostly in CuCrZr SAA). It should be noted that the *J–R* data in this study do not satisfy the validity requirements of the ASTM standards. The J_Q values were taken as either the maximum when the *J–R* data are still on blunting line, or were estimated by the intersection of the regression line with the 0.2-mm offset line on the *J–R* curves. While the fracture toughness data are invalid according to the ASTM standard, the obtained J_Q values well reflect the trend of changes in the material's toughness when the same specimen geometry and test technique are applied. Fracture toughness data did not show an apparent correlation with tensile property data. In particular, the significant irradiation hardening together with dramatic loss of strain hardening ability and uniform elongation in both irradiated CuCrZr SAA and CuCrZr SCA did not lead to a marked decrease in fracture toughness. Though inconclusive, both unirradiated and irradiated CuCrZr SCA seems to have relatively lower fracture toughness than CuCrZr SAA.

4.3. Effect of strain rate on irradiation hardening

The strain rate dependence of tensile properties has been investigated in this work for both unirradiated and irradiated CuCrZr. The strain rate sensitivity is small at room temperature in unirradiated CuCrZr, which is consistent with previous studies by Zinkle et al. [27] and Edwards [33]. The measured strain rate sensitivity parameter, m is <0.01 for CuCrZr SAA and ~0.01 for CuCrZr SCA, where $\sigma_y = C\dot{\varepsilon}^m$ and C is a constant. Zinkle et al. reported m = ~0.01 for unirradiated CuCrZr SAA [27]. No data on the strain rate dependence in irradiated CuCrZr can be found in the open literature. Due to significant hardening and loss of ductility following irradiation, it is interesting to see if neutron irradiation changes the strain rate dependence of tensile properties. A small increase in strain-rate dependence of the yield stress was observed in CuCrZr SCA with a higher yield stress at higher strain rate. The strain rate sensitivity parameter increased to ~0.02 in CuCrZr SAA after neutron irradiation to 1.5 dpa. Zinkle et al. [34] observed a small strain rate dependence of tensile strength in GlidCop Al15 and MAGT 0.2 grades of oxide dispersion strengthened copper neutron-irradiated to ~13 dpa at 200 °C with $m \sim 0.02$ for GlidCop Al15 and $m < 0.01$ for MAGT 0.2. In general, the strain rate and temperature dependence of flow stresses is small in fcc metals. Neutron irradiation can increase the dependence of the flow stresses for fcc metals due to a change in thermally-activated deformation mechanism [35].

5. Summary and conclusions

The effect of neutron irradiation on tensile and fracture toughness properties of CuCrZr after two heat treatments was investigated. The two heat treatments were (1) solution-annealed, water quenched and aged (CuCrZr SAA), and (2) HIPped, solution-annealed with a slow cooling rate and aged (CuCrZr SCA). The second heat treatment simulated the manufacturing cycle for ITER large components. The tensile strength and tensile elongation of CuCrZr SCA are significantly lower than those of CuCrZr SAA. For both heat treatments, yield stress increased significantly with increasing dose, with a saturation dose of ~0.1 dpa. Plastic instability at yield (decrease of uniform elongation to a very low value) also occurred at ~0.1 dpa. The effect of neutron irradiation on tensile behavior of CuCrZr SAA and CuCrZr SAC was similar with minor differences that perhaps are attributable to the precipitate microstructure.

The yield stresses for unirradiated CuCrZr SAA and CuCrZr SCA were insensitive to the strain rate. Neutron irradiation introduced significant hardening in the two alloy conditions, while the dependence of the yield stress on the strain rate was only slightly affected by neutron irradiation.

The heat treatments had no significant influence on fracture toughness of unirradiated CuCrZr. Neutron irradiation slightly reduced the fracture toughness for both CuCrZr SAA and CuCrZr SCA, though the fracture toughness of CuCrZr remained high up to ~1.5 dpa (J_Q > 200 kJ/m^2).

Acknowledgements

The research was sponsored by the Office of Fusion Energy Sciences, the US Department of Energy under Contract DE-AC05-00OR22725 with Oak Ridge National Laboratory, managed and operated by UT-Battelle, LLC. Dr Alan Peacock at EFDA Close Support Unit in Garching, Germany provided the materials. The authors would like to thank E.T. Manneschmidt, R. Swain and D.A. McClintock and L.T. Gibson for their technical support.

References

[1] V. Barabash et al., The ITER International Team, J. Nucl. Mater. 367–370 (2007) 21.
[2] ITER Materials Properties Handbook Ed. 2006, internal distribution.
[3] S.J. Zinkle, S.A. Fabritsiev, Nuclear Fusion Supplement (Material Properties Data Compendium for Fusion Plasma Facing Components), vol. 5 (1994) p. 163.
[4] G.J. Butterworth, C.B.A. Forty, J. Nucl. Mater. 189 (1992) 237.
[5] S.J. Zinkle, W.S. Eatherly, Fusion Materials Semi-annual Progress Report DOE/ER-0313/22, Oak Ridge National Laboratory, June 1997, p. 143.
[6] U. Holzwarth, M. Pisoni, R. Scholz, H. Stamm, A. Volcan, J. Nucl. Mater. 279 (2000) 19.
[7] D.J. Edwards, B.N. Singh, S. Tahtinen, J. Nucl. Mater. 367–370 (2007) 904.
[8] A.D. Ivanov, A.K. Nikolaev, G.M. Kalinin, M.E. Rodin, J. Nucl. Mater. 307–311 (2002) 673.
[9] G. Kalinin, V. Barabash, A. Cardella, et al., J. Nucl. Mater. 283–287 (2000) 10.
[10] S.A. Fabritsiev, S.J. Zinkle, B.N. Singh, J. Nucl. Mater. 283–287 (2000) 127.
[11] L. Briottet, I. Chu, P. Lemoine, H. Giraud, Optimization of One Step SS/SS and SS/CuCrZr HIP Joints for Retainment of CuCrZr Properties, Report Technique DTEN/DL/2003/028, CEA Grenoble, 2003.
[12] A.F. Rowcliffe, ITER US Home Team Final Report for G16 TT71(T213), 1998.
[13] R. Suzuki, M. Saito, T. Hatano, Fus. Sci. Technol. 44 (2003) 242.

[14] O. Gillian, I. Chu, P. Lemoine, Characterisation of the CuCrZr/SS Junction Strength for Different Blanket Manufacturing Conditions, Final Report. CEA Grenoble, France, Rapport Technique DTEN/DL/2005/027, 2005.
[15] T. Hatano, M. Enoeda, T. Kuroda, M. Akiba, Development of HIP Technique for Bonding of CuCrZr with Stainless Steel and Beryllium for Application to the ITER First Wall, October 2002, 67p. Report Number: JAERI-ch–2002-075 Japan Atomic Energy Research Inst., Tokyo, Japan.
[16] S. Tahtinen, M. Pyykkonen, P. Karjalainen-Roikonen, B.N. Singh, P. Toft, J. Nucl. Mater. 258–263 (1998) 1010.
[17] S. Tahtinen, M. Pyykkonen, B.N. Singh, P. Toft, in: M.L. Hamilton et al. (Eds.), 19th International Symposium on Effects of Radiation on Materials, ASTM STP 1366 (American Society for Testing and Materials, West Conshohocken, PA, 2000), p. 1243.
[18] D.J. Alexander, S.J. Zinkle, A.F. Rowcliffe, J. Nucl. Mater. 271&272 (1999) 429.
[19] Standard Test Method for Measurement of Fracture Toughness, Designation E1820-06, Annual Book of ASTM Standards, vol. 03.01.
[20] R.K. Nanstad, D.J. Alexander, R.L. Swain, J.T. Hutton, D.L. Thomas, ASTM STP 1092, in: A.A. Braun, N.E. Ashbaugh, F.M. Smith (Eds.), American Society for Testing and Materials, Philadelphia, 1990, p. 7.
[21] D.J. Alexander, ASTM STP 1204, in: W.R. Corwin, F.M. Haggag, W.L. Server (Eds.), American Society for Testing and Materials, Philadelphia, 1993, p. 130.
[22] D.J. Edwards, B.N. Singh, Q. Xu, P. Toft, J. Nucl. Mater. 307–311 (2002) 439.
[23] B.N. Singh, D.J. Edwards, M. Eldrup, P. Toft, J. Nucl. Mater. 249 (1997) 1.
[24] D.J. Edwards, B.N. Singh, P. Toft, M. Eldrup, J. Nucl. Mater. 258–263 (1998) 978.
[25] Z. Rdzawski, J. Stobrawa, Script. Metall. 20 (1986) 341.
[26] K. Farrell, Dimensional Stability and Mechanical Behavior of Irradiated Metals and Alloys, vol. 1, British Nuclear Energy Society, London, 1983, p. 73.
[27] S.J. Zinkle, W.S. Eatherly, Fusion Materials Semi-annual Progress Report DOE/ER-0313/21, Oak Ridge National Laboratory, December 1996, p. 165.
[28] T. Toda, Trans. Japan Inst. Met. 11 (1970) 24.
[29] T. Toda, Trans. Japan Inst. Met. 11 (1970) 30.
[30] H. Suzuki, M. Kanno, Trans. Japan Inst. Met. 35 (1971) 434.
[31] P. Jung, A. Hishinuma, G.E. Lucas, H. Ullmaier, J. Nucl. Mater. 232 (1996) 186.
[32] D.J. Edwards, Fusion Materials Semi-annual Progress Report DOE/ER-0313/39, Oak Ridge National Laboratory, December 2005, p. 85.
[33] D.J. Edwards, Fusion Materials Semi-annual Progress Report DOE/ER-0313/25, Oak Ridge National Laboratory, December 1998, p. 185.
[34] S.J. Zinkle, L.T. Gibson, Fusion Materials Semi-annual Progress Report DOE/ER-0313/27, Oak Ridge National Laboratory, December 1999, p. 163.
[35] T.H. Blewitt, T.J. Koppenaal, in: W.F. Sheely (Ed.), AIME Symposium on Radiation Effects, Asheville, NC, (Metallurgical Society Conference, vol. 37), Gordon and Breach, New York, 1967, p. 561.